pharmaceutics

MDPI

Article

A Finite Element Method for Modeling Diffusion and Drug Release from Nanocellulose/Nanoporous Silicon Composites

Paulo Zúñiga [1,*], Marcelo Aravena [1], Silvia Ponce [2] and Jacobo Hernandez-Montelongo [1,3,*]

[1] Department of Mathematical and Physical Sciences, Catholic University of Temuco, Temuco 4813302, Chile; maravena2021@alu.uct.cl
[2] Institute of Scientific Research IDIC, University of Lima, Lima 15023, Peru; sponce@ulima.edu.pe
[3] Department of Chemical Engineering, University of Guadalajara, Guadalajara 44430, Mexico
* Correspondence: paulo.zuniga@uct.cl (P.Z.); jacobo.hernandez@uct.cl (J.H.-M.)

Abstract: Background and Objective: A previous study investigated the in vitro release of methylene blue (MB), a widely used cationic dye in biomedical applications, from nanocellulose/nanoporous silicon (NC/nPSi) composites under conditions simulating body fluids. The results showed that MB release rates varied significantly with the nPSi concentration in the composite, highlighting its potential for controlled drug delivery. To further analyze the relationship between diffusion dynamics and the MB concentration, this study developed a finite element (FE) method to solve Fick's equations governing the drug delivery system. **Methods**: Release profiles of MB from NC/nPSi composites with varying nPSi concentrations (0%, 0.1%, 0.5%, and 1.0%) were experimentally measured in triplicate using phosphate-buffered saline (PBS) at 37 °C, pH 7.4, and 100 rpm. Mathematical models incorporating linear and quadratic dependencies of the diffusion coefficient on the MB concentration were developed and tested using the FE method. Model parameters were refined by minimizing the error between simulated and experimental MB release profiles. **Results**: The proposed FE method closely matched experimental data, validating its accuracy and robustness in simulating the diffusion and release processes. **Conclusions**: This study emphasizes the significant impact of the nPSi concentration on enhancing release control and highlights the importance of material composition in designing drug delivery systems. The findings suggest that the FE method can be effectively applied to model other complex systems, paving the way for advancements in precision drug delivery and broader biomedical applications.

Keywords: finite element method; drug delivery; composites; nanocellulose; nanoporous silicon

Academic Editor: Fjóla Jónsdóttir

Received: 15 December 2024
Revised: 9 January 2025
Accepted: 13 January 2025
Published: 16 January 2025

Citation: Zúñiga, P.; Aravena, M.; Ponce, S.; Hernandez-Montelongo, J. A Finite Element Method for Modeling Diffusion and Drug Release from Nanocellulose/Nanoporous Silicon Composites. *Pharmaceutics* **2025**, *17*, 120. https://doi.org/10.3390/pharmaceutics17010120

1. Introduction

Nanoporous silicon (nPSi) stands out as an excellent biomaterial for drug delivery applications due to its high surface area, biocompatibility, biodegradability, and bioresorbability [1–3]. Typically, drugs are either loaded into the porous matrix or immobilized on the surface following appropriate surface derivatization. When combined with biopolymers, it acts as a substrate for composite materials, introducing advantageous chemical and physical properties not present in individual components. These benefits include improved control over drug release kinetics and enhanced stability in aqueous solutions [4,5]. As a result, nPSi has been paired with various organic matrices to create composites as advanced drug delivery systems, such as β-cyclodextrin polymers [4,6,7], oxidized hyaluronic acid hydrogels [8], and poly(L-lactide) acid [9], among others.

In this context, nanocellulose (NC) has recently emerged as one of the most promising "green" materials for obtaining drug delivery carriers as composites. It offers adaptable surface chemistry, a high surface area, biocompatibility, and biodegradability [10,11]. Recently, K. Garrido-Miranda et al. [12] synthesized NC/nPSi composites for the controlled release of methylene blue (MB), a cationic thiazine dye widely used in biomedicine for various purposes. These include the treatment of methemoglobinemia [13], its use as a marker and indicator in various surgical techniques [14], and its use as an analgesic in different treatments [15]. Additionally, it has been applied as an antibacterial, antiviral agent, and against cancer cells [16].

On the other hand, the finite element (FE) method is a numerical technique commonly used to approximate the solution of ordinary and partial differential equations (see, e.g., [17–19] and the references therein). It involves writing the equation in its variational (weak) form and approximating the solution, originally defined in an infinite-dimensional space, by restricting it to a finite-dimensional subspace. This approach has been successfully applied to simulate various physical phenomena, including the fluid–structure interaction [20], electromagnetism [21], and heat transfer [22].

This work presents an FE method to simulate the diffusion and controlled release of MB from NC/nPSi composites. The simulations are based on Fick's second law [23], a widely used model for release kinetics (e.g., [24–28]). In this study, a concentration-dependent diffusion coefficient is incorporated to more accurately represent the behavior of highly polymerized NC. Furthermore, the influence of temperature on diffusivity in biological environments is considered a critical factor. This temperature dependency is modeled using the Stokes–Einstein relationship [29], offering a deeper insight into the dynamics of the diffusion process:

$$D = \frac{k_B T}{a \eta r},$$

where k_B is Boltzmann's constant, T represents the temperature, a denotes the viscosity, η is a constant that accounts for the boundary conditions between the diffusing molecule and the solvent, and r is the radius of the molecule. Consequently, diffusion coefficients increase with temperature, as observed in drug delivery experiments [30,31].

Nevertheless, as this model is further refined by incorporating dependency relations from [32], which align with the experimental release profiles reported by K. Garrido-Miranda et al. [12], the influence of temperature was not investigated and remains limited to a concentration-dependent diffusion coefficient.

Fick's second law is first discretized using the FE method, transforming the governing equation into a discrete system. Since the diffusion coefficient depends on concentration, the non-linearities are addressed using the Picard iteration. This method linearizes the system at each time step, enabling its resolution using Octave [33]. The proof of unique solvability of the system is provided under the assumption of a bounded diffusion coefficient. Based on this assumption, examples are presented to offer valuable insights into designing more efficient drug delivery systems for biomedical applications.

The outline of this article is as follows. Section 2 presents the model problem and its FE discretization. A case study comparing the numerical solution with experimental data is presented in Section 3. Numerical details concerning future directions are discussed in Section 4, while conclusions are drawn in Section 5.

2. Materials and Methods

2.1. Model Problem

This work is about the one-dimensional diffusion and controlled release of MB through an NC/nPSi composite of thickness $2L$ (see Figure 1). It is assumed that L is sufficiently small, such that the amount of MB passing through the edges of the composite is negligible.

In this context, the drug delivery system is modeled within the framework of Fick's second law [23], a widely used approach in diffusion processes, with a diffusion coefficient D that depends on the concentration ϕ. Let $I = (-L, L)$ be an interval along the x-axis, and let $T > 0$ be a given finite time. The governing equation is

$$\frac{\partial \phi}{\partial t} = \frac{\partial}{\partial x}\left(D(\phi)\frac{\partial \phi}{\partial x}\right) \quad \text{in} \quad I \times (0, T). \tag{1}$$

At the surfaces $x = \pm L$, the concentration is prescribed as $\phi = \phi_\infty$ for all $t \in (0, T)$.

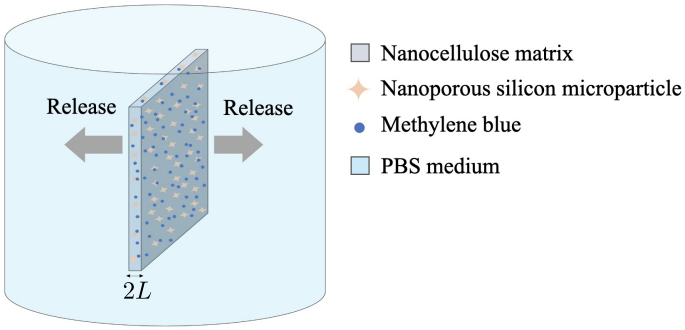

Figure 1. Scheme of the drug delivery system.

When the concentration is initially uniform, with $\phi(x, 0) = \phi_0$ for all $x \in I$, and both D and ϕ_∞ are constants, the partial differential Equation (1) can be solved using the method of separation of variables or the Laplace transform, as detailed in [34]. This gives

$$\frac{\phi(x,t) - \phi_0}{\phi_\infty - \phi_0} = 1 - \frac{4}{\pi}\sum_{n=0}^{\infty}\frac{(-1)^n}{(2n+1)}\cos\left[\frac{(2n+1)\pi x}{2L}\right]\exp\left[-\frac{D(2n+1)^2\pi^2 t}{4L^2}\right]. \tag{2}$$

Moreover, if M_t denotes the amount of MB released at time t and M_∞ the corresponding quantity after infinite time, the release profile is given by

$$\frac{M_t}{M_\infty} = 1 - \frac{8}{\pi^2}\sum_{n=0}^{\infty}\frac{1}{(2n+1)^2}\exp\left[-\frac{D(2n+1)^2\pi^2 t}{4L^2}\right]. \tag{3}$$

Although assuming a constant D is common in diffusion modeling, this assumption is unrealistic for highly polymerized substances [34], such as NC and NC-based composites. Given the relevance of the NC in this context, Fick's second law in (1) with a variable D will be addressed in the following sections, focusing on the numerical solution. To facilitate understanding, we first analyze the case with a constant D and then extend the analysis to accommodate $D = D(\phi)$.

2.2. Constant Diffusion Coefficient

2.2.1. Preliminaries

Let us review some basic concepts of functional analysis which are useful in dealing with partial differential equations. We first define the Sobolev space $H^1(I)$ as

$$H^1(I) := \{\psi \in L^2(I) : \ \psi' \in L^2(I)\},$$

which is a Hilbert space equipped with the inner product

$$(\phi, \psi)_{1,I} := \int_I \phi\psi \, \mathrm{d}x + \int_I \phi'\psi' \, \mathrm{d}x \qquad \forall \phi, \psi \in H^1(I).$$

For further details, we refer the reader to [35]. The norm induced by $(\cdot,\cdot)_{1,I}$ is given by

$$\|\psi\|_{1,I} := \left(\|\psi\|_{0,I}^2 + |\psi|_{1,I}^2\right)^{1/2} \qquad \forall \psi \in H^1(I),$$

where $|\psi|_{1,I} := \|\psi'\|_{0,I}$ is a semi-norm on $H^1(I)$. It is well known that the quantity $|\psi|_{1,I}$ is a norm equivalent to $\|\psi\|_{1,I}$ on the following subspace of $H^1(I)$:

$$H_0^1(I) := \left\{\psi \in H^1(I) : \ \psi = 0 \quad \text{at} \quad x = \pm L\right\}, \tag{4}$$

due to Poincaré's inequality. This result is stated below, and its proof can be found in ([35], Proposition 8.13).

Lemma 1 (Poincaré's inequality)**.** *Let I be a bounded interval. Then, there exists a constant $C_P > 0$, depending only on I, such that*

$$\|\psi\|_{1,I} \leq C_P |\psi|_{1,I} \qquad \forall \psi \in H_0^1(I). \tag{5}$$

Finally, we note that an alternative way of interpreting ϕ in (1) is to treat it as a function of time, taking values in a Sobolev space, e.g., V, where the elements of V are functions that depend only on the spatial variable:

$$\phi : t \in (0, T) \mapsto \phi(t) \equiv \phi(\cdot, t) \in V.$$

This notation will be used throughout this work. Furthermore, time derivatives will be denoted by $d_t(\cdot)$.

2.2.2. Weak Formulation

To introduce the weak formulation of Fick's second law, we multiply (1) by a test function $\psi \in H_0^1(I)$, assume a constant D, and perform integration over I, yielding

$$\int_{-L}^{L} \psi d_t \phi(t) \, \mathrm{d}x + D \int_{-L}^{L} \phi'(t)\psi' \, \mathrm{d}x - D\phi'(t)\psi \Big|_{x=-L}^{x=L} = 0.$$

Then, using the condition that $\psi = 0$ at $x = \pm L$ (cf. (4)), we obtain

$$\int_{-L}^{L} \psi d_t \phi(t) \, \mathrm{d}x + D \int_{-L}^{L} \phi'(t)\psi' \, \mathrm{d}x = 0. \tag{6}$$

By virtue of identity (6) and under the conditions used to determine the exact ϕ in (2), the weak formulation of Equation (1) with a constant D reads the following: For almost every $t \in (0, T)$, find $\phi(t) \in H^1(I)$, such that $\phi = \phi_\infty$ on $\{-L, L\} \times (0, T)$, $\phi = \phi_0$ on $I \times \{0\}$, and

$$\int_{-L}^{L} \psi d_t \phi(t) \, \mathrm{d}x + D \int_{-L}^{L} \phi'(t)\psi' \, \mathrm{d}x = 0 \qquad \forall \psi \in H_0^1(I). \tag{7}$$

At this point, we emphasize that the FE method, which will be detailed later, does not directly allow us to deduce the unique solvability for the discretization of (7) when $\phi_\infty \neq 0$. This is because, in this case, the discrete versions of $\phi(t)$ and ψ reside in different

spaces. To address this issue, we recall that the orthogonal complement of $H_0^1(I)$ in $H^1(I)$ is defined by

$$H_0^1(I)^\perp := \left\{ \lambda \in H^1(I) : \ (\lambda, \psi)_{1,I} = 0 \quad \forall\, \psi \in H_0^1(I) \right\}. \tag{8}$$

It follows that $\lambda \in H_0^1(I)^\perp$ if and only if λ is the weak solution to the equation

$$-\lambda'' + \lambda = 0.$$

Accordingly, we decompose $H^1(I)$ as the direct sum $H_0^1(I) \oplus W$, where W is the subspace spanned by $\{e^x, e^{-x}\}$. Next, we introduce the auxiliary unknown

$$\vartheta(t) := \phi(t) - \lambda, \tag{9}$$

with $\lambda \in H_0^1(I)^\perp$ being defined by

$$\lambda(x) := \left(\frac{\phi_\infty}{e^L + e^{-L}} \right) (e^x + e^{-x}). \tag{10}$$

It is easy to check that $\lambda(-L) = \lambda(L) = \phi_\infty$, from which we deduce that (7) is equivalent to the following problem: for almost every $t \in (0, T)$, find $\vartheta(t) \in H_0^1(I)$ such that $\vartheta = \phi_0$ on $I \times \{0\}$ and

$$\int_{-L}^{L} \psi d_t \vartheta(t)\, \mathrm{d}x + D \int_{-L}^{L} \vartheta'(t)\psi'\, \mathrm{d}x = -D \int_{-L}^{L} \lambda'\psi'\, \mathrm{d}x \qquad \forall\, \psi \in H_0^1(I). \tag{11}$$

We can therefore use ϑ to recover the solution to (7). In particular, $\vartheta = \phi$ when $\phi_\infty = 0$.

2.3. Discretization of the Model with a Constant Diffusion Coefficient

This section focuses on approximating the solution to (11) using a fully discrete scheme that combines an FE method in space with an implicit Euler method in time. For simplicity, homogeneous boundary conditions are initially assumed. The non-homogeneous case will be addressed in Section 2.3.3.

2.3.1. Fully Discrete Scheme

Let V_h denote an arbitrary finite-dimensional subspace of $H_0^1(I)$. We begin by considering the problem given by (11) with $\phi_\infty = 0$. We discretize this problem in space using the following FE scheme: For each $t \in [0, T]$, find $\vartheta_h(t) \in V_h$ such that $\vartheta_h^0 = \phi_h^0$ and

$$\int_{-L}^{L} \psi_h d_t \vartheta_h(t)\, \mathrm{d}x + A(t, \vartheta_h, \psi_h) = 0 \qquad \forall\, \psi_h \in V_h, \tag{12}$$

where the bilinear form $A : t \mapsto H_0^1(I) \times H_0^1(I)$ is defined by

$$A(t, \vartheta_h, \psi_h) := D \int_{-L}^{L} \vartheta_h'(t)\psi_h'\, \mathrm{d}x, \tag{13}$$

and ϕ_h^0 is the L^2-projection of ϕ_0 into V_h, such that $\phi_h^0 \in V_h$ satisfies, for all $\psi_h \in V_h$,

$$\int_{-L}^{L} \phi_h^0 \psi_h\, \mathrm{d}x = \int_{-L}^{L} \phi_0 \psi_h\, \mathrm{d}x. \tag{14}$$

To discretize in time, we partition the interval $[0, T]$ as

$$0 = t^0 < t^1 < \cdots < t^{N+1} = T,$$

with time step denoted by $\Delta t^n := t^{n+1} - t^n$ for $n \in \{0, 1, \ldots, N\}$. Furthermore, we denote a function $\zeta(t)$ at time level $t = t^n$ by ζ^n.

For the implicit Euler method in time, we use

$$(d_t \vartheta_h)^{n+1} \approx \frac{\vartheta_h^{n+1} - \vartheta_h^n}{\Delta t^n}.$$

Inserting this expression into (12) at time t^{n+1} yields the following fully discrete formulation of (11) with homogeneous boundary conditions: For each $n \in \{0, 1, \ldots, N\}$, find $\vartheta_h^{n+1} \in V_h$, such that

$$B(\vartheta_h^{n+1}, \psi_h) + \Delta t^n A(\vartheta_h^{n+1}, \psi_h) = B(\vartheta_h^n, \psi_h) \qquad \forall\, \psi_h \in V_h, \tag{15}$$

where, for easy of notation, we write $A(\vartheta_h^{n+1}, \psi_h)$ instead of $A(t^{n+1}, \vartheta_h^{n+1}, \psi_h)$ and

$$B(\vartheta_h, \psi_h) := \int_{-L}^{L} \phi_h \psi_h \, \mathrm{d}x \qquad \forall\, \vartheta_h, \psi_h \in V_h. \tag{16}$$

We will show that problem (15) reduces to a system of linear equations. To achieve this, we assume that $M = \dim V_h < \infty$ and let $\{e_1, \ldots, e_M\}$ be a basis of V_h. Then, for each $n \in \{0, 1, \ldots, N\}$, there exist $\alpha_1^{n+1}, \ldots, \alpha_M^{n+1} \in \mathbb{R}$ such that

$$\vartheta_h^{n+1} = \sum_{j=1}^{M} \alpha_j^{n+1} e_j. \tag{17}$$

We therefore write (15) as follows: For each $n \in \{0, 1, \ldots, N\}$, find $\alpha_1^{n+1}, \ldots, \alpha_M^{n+1} \in \mathbb{R}$ such that

$$\sum_{j=1}^{M} \alpha_j^{n+1} \left\{ B(e_j, e_i) + \Delta t^n A(e_j, e_i) \right\} = \sum_{j=1}^{M} \alpha_j^n B(e_j, e_i) \qquad \forall\, i = 1, \ldots, M. \tag{18}$$

In this way, if we set $a_{ij} := A(e_j, e_i)$ and $b_{ij} := B(e_j, e_i)$, so that

$$\alpha^{n+1} := (\alpha_j^{n+1}) \in \mathbb{R}^M, \quad \mathsf{A} := (a_{ij}) \in \mathbb{R}^{M \times M}, \quad \mathsf{B} := (b_{ij}) \in \mathbb{R}^{M \times M},$$

the matrix form of (18) reads the following: For each $n \in \{0, 1, \ldots, N\}$, find $\alpha^{n+1} \in \mathbb{R}^M$, which satisfies

$$(\mathsf{B} + \Delta t^n \mathsf{A}) \alpha^{n+1} = \mathsf{B} \alpha^n, \tag{19}$$

where the iteration is initialized with $\alpha^0 \in \mathbb{R}^M$ obtained from (14). The following result establishes the unique solvability of the linear system (19).

Theorem 1. *The matrix* $\mathsf{B} + \Delta t^n \mathsf{A}$ *is symmetric and positive definite, and therefore invertible.*

Proof. The symmetry property follows directly from the definition of the bilinear forms A and B. Next, given $\beta := (\beta_j) \in \mathbb{R}^M$, we set

$$\psi_h = \sum_{j=1}^{M} \beta_j e_j. \tag{20}$$

Proceeding analogously to ([36], Chapter 4), that is, using the $H_0^1(I)$-ellipticity of the form A with ellipticity constant $C > 0$, depending on the diffusion coefficient D and the constant from Poincaré's inequality (cf. (5)), we obtain

$$\beta^{\mathrm{T}}(\mathsf{B} + \Delta t^n \mathsf{A})\beta = \sum_{i,j=1}^{M} (b_{ij} + \Delta t^n a_{ij})\beta_i\beta_j = B(\psi_h, \psi_h) + \Delta t^n A(\psi_h, \psi_h)$$
$$\geq \|\psi_h\|_{0,I}^2 + \Delta t^n C\|\psi_h\|_{1,I}^2 \geq \Delta t^n C\|\psi_h\|_{1,I}^2.$$

Since $\beta^{\mathrm{T}}(\mathsf{B} + \Delta t^n \mathsf{A})\beta > 0$ for all β values that are different from the null vector, the result follows. □

2.3.2. Specific FE Subspace

This section specifies the matrix structure of the linear system (19) for a particular choice of V_h. Let $\{x_m\}_{0 \leq m \leq M+1}$ be a uniform partition of the interval $\bar{I} = [-L, L]$, with the meshsize being denoted by $h > 0$. We set

$$V_h = \left\{ \psi_h \in C(\bar{I}) : \ \psi_h\Big|_{[x_{j-1}, x_j]} \in \mathcal{P}_1([x_{j-1}, x_j]) \quad \forall\, j = 1, \cdots, M+2 \right\} \cap H_0^1(I), \tag{21}$$

where $\mathcal{P}_1(S)$ denotes the space of polynomials of degree ≤ 1 defined over an interval S.

The following definition can be found in ([37], Section 1.1.2).

Definition 1. *For each $i \in \{1, \ldots, M\}$, the hat functions $e_i \in V_h$ are defined as*

$$e_i(x) = \begin{cases} \dfrac{x - x_{i-1}}{h} & x \in [x_{i-1}, x_i], \\ \dfrac{x_{i+1} - x}{h} & x \in [x_i, x_{i+1}], \\ 0 & x \notin [x_{i-1}, x_{i+1}]. \end{cases}$$

An example of a hat function is shown in Figure 2. It follows that $e_i(x_j) = \delta_{ij}$, where δ_{ij} is the Kronecker delta function. Moreover, $\{e_1, \ldots, e_M\}$ is a basis for V_h; hence, a function $\psi_h \in V_h$ is uniquely determined by the values $\{\psi_h(x_i)\}_{1 \leq i \leq M}$, namely

$$\psi_h = \sum_{i=1}^{M} \psi_h(x_i) e_i.$$

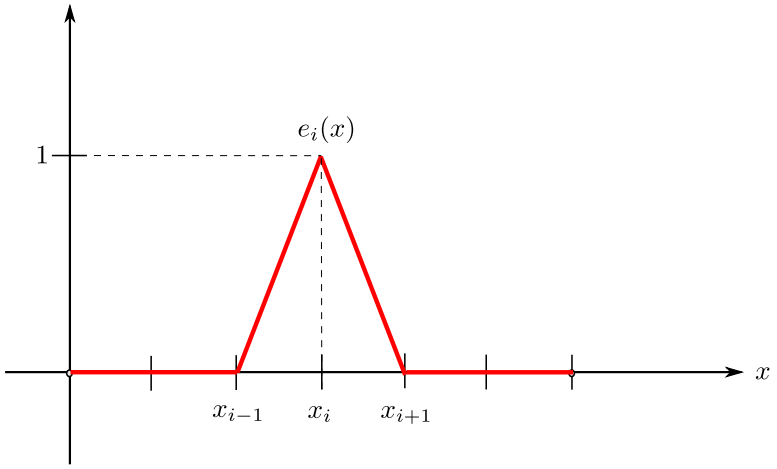

Figure 2. Example of hat function.

Note that $a_{ij} = b_{ij} = 0$ when $|i - j| \geq 2$. Furthermore, we obtain, after some algebraic manipulations,

$$a_{ij} = \begin{cases} \dfrac{2D}{h} & \text{if } j = i, \\ -\dfrac{D}{h} & \text{if } |j - i| = 1. \end{cases}$$

Similarly,

$$b_{ij} = \begin{cases} \dfrac{2h}{3} & \text{if } j = i, \\ \dfrac{h}{6} & \text{if } |j - i| = 1. \end{cases}$$

Consequently, the global matrix of (19) is tridiagonal, which is highly desirable in situations where the dimension of V_h is very large, as this allows for a reduction in the number of *flop* required to solve the system. In particular, a tridiagonal system can be solved using the Thomas algorithm, which requires significantly fewer *flop* than the method that directly computes the inverse of the matrix. For further details, we refer the reader to [38].

2.3.3. Numerical Treatment of Non-Homogeneous Boundary Conditions

Recall from (9) that the unknowns ϕ and ϑ are related by the decomposition $\phi = \vartheta + \lambda$, where λ is defined such that $\lambda = \phi_\infty$ at $x = \pm L$. This approach allows ϕ to be recovered from ϑ, even in the presence of non-homogeneous boundary conditions. Building on this idea, we approximate ϕ using the decomposition

$$\phi_h^{n+1} = \vartheta_h^{n+1} + \lambda_h, \qquad n \in \{0, 1, \ldots, N\}, \tag{22}$$

where $\vartheta_h^{n+1} \in V_h$ is given by (17), with V_h being defined in (21), and λ_h is a polynomial satisfying the boundary conditions $\lambda_h(-L) = \lambda_h(L) = \phi_\infty$. Specifically, we define

$$\lambda_h := \phi_\infty(e_0 + e_{M+1}), \tag{23}$$

where e_0 and e_{M+1} are the hat functions associated with the endpoints of I.

Next, using the same notation as in Section 2.3.2, the fully discrete formulation of (11) reads as follows: for each $n \in \{0, 1, \ldots, N\}$, find $\vartheta_h^{n+1} \in V_h$ such that $\vartheta_h^0 = \phi_h^0$ (cf. (14)) and

$$B(\vartheta_h^{n+1}, \psi_h) + \Delta t^n A(\vartheta_h^{n+1}, \psi_h) = B(\phi_h^n, \psi_h) - \Delta t^n D \int_{-L}^{L} \lambda_h' \psi_h' \, \mathrm{d}x \qquad \forall\, \psi_h \in V_h. \tag{24}$$

It is clear that (24) coincides with (15) when $\phi_\infty = 0$.

Now let $\mu \in \mathbb{R}^M$ be the vector whose entries are all zero, except for the first and last ones, which are both set to ϕ_∞. Then, for each $n \in \{0, 1, \ldots, N\}$, the discretization (24) yields

$$(\mathsf{B} + \Delta t^n \mathsf{A})\alpha^{n+1} = \mathsf{B}\alpha^n - \Delta t^n \mathsf{A}\mu. \tag{25}$$

Here, the matrices A and B are defined as in Section 2.3.2, thus ensuring the unique solvability of the linear system (25), which follows directly from Theorem 1.

We end this section by noting that the discrete concentration with non-homogeneous boundary conditions can be computed from (22) using the solution of (25), which provides

$$\phi_h^{n+1} = \sum_{j=0}^{M+1} \alpha_j^{n+1} e_j, \qquad n \in \{0, \ldots, N\},$$

with $\phi_h^{n+1}(-L) = \phi_h^{n+1}(L) = \phi_\infty$, as required.

2.4. Variable Diffusion Coefficient

This section presents an FE method to solve the non-linear equation in (1), assuming ϕ_∞ is time-dependent for greater generality. Although this model is more challenging to analyze with FE methods due to the concentration dependence of D, it still relies on the previous results.

The weak form of (1) resembles (11), with the form A now replaced by

$$A(\phi;\vartheta,\psi) := \int_{-L}^{L} D(\phi(t))\vartheta'(t)\psi' \,\mathrm{d}x \qquad \forall\, \psi \in H_0^1(I).$$

Note here that $\vartheta(t) := \phi(t) - \lambda(t)$ and $\lambda(t) \in H_0^1(I)^\perp$ with $\lambda(t) = \phi_\infty(t)$ at $x = \pm L$.

Proceeding analogously to Section 2.3, we discretize the weak formulation of (1) using an FE method in space and an implicit Euler method in time. To handle the non-linearities, we employ a Picard-type iteration. Specifically, we consider the following fully discrete scheme: for each $n \in \{0, 1, \ldots, N\}$ and given ϕ_h^n, find $\vartheta_h^{n+1} \in V_h$ such that $\vartheta_h^0 = \phi_h^0$ and

$$\begin{aligned} &B(\vartheta_h^{n+1}, \psi_h) + \Delta t^n A(\phi_h^n; \vartheta_h^{n+1}, \psi_h) \\ &\qquad = B(\vartheta_h^n, \psi_h) - \int_{-L}^{L} \lambda_h^{n+1}\psi_h \,\mathrm{d}x - \Delta t^n \int_{-L}^{L} D(\phi_h^n)(\lambda_h^{n+1})'\psi_h' \,\mathrm{d}x \qquad \forall\, \psi_h \in V_h, \end{aligned} \tag{26}$$

where ϕ_h^0 is given by (14) and B by (16). Furthermore, the last two integrals in (26) arise from the treatment of the time-dependent boundary condition. In fact, proceeding as in Section 2.3.3, we obtain

$$\phi_h^{n+1} = \vartheta_h^{n+1} + \lambda_h^{n+1}, \quad \text{with} \quad \lambda_h^{n+1} := \phi_\infty^{n+1}(e_0 + e_{M+1}). \tag{27}$$

Now, inspired by [32], we define

$$D(\phi) := D_0(1 + \delta\phi)^k, \tag{28}$$

where $k \in \mathbb{N}$, $\delta \in \mathbb{R}$, and $D_0 > 0$ are experimentally determined constants. For the sake of simplicity, we assume that k is either 1 or 2. However, the analysis in this section can be easily extended to cases where $k > 2$. We furthermore assume that D is bounded: There exists a constant $D_* > 0$ such that, for all $\psi \in [0, 1]$,

$$D(\psi) \geq D_*. \tag{29}$$

Remark 1. *As discussed in [39], a general form for the diffusion coefficient is $D(\phi) = D_0F(\phi)$, where $D_0 = D(0)$ is a positive constant. The choice in (28), with $F(\phi) = (1 + \delta\phi)^k$, represents a specific instance of this general form. While other forms of F, such as exponential functions, have been explored in the literature (see, e.g., [40]), we restrict our focus to (28) for brevity.*

Next, we specify the matrix form of the fully discrete scheme (26), subjected to the diffusion coefficient (28). Let $\hat{\mathsf{A}} := (\hat{a}_{ij}) \in \mathbb{R}^{M\times M}$ denote the matrix given by

$$\hat{a}_{ij} := A(\phi_h^n; e_j, e_i) = \int_{-L}^{L} D(\phi_h^n)e_i'e_j' \,\mathrm{d}x = D_0 \int_{-L}^{L} \left(1 + \delta \sum_{l=0}^{M+1} \alpha_l^n e_l\right)^k e_i'e_j' \,\mathrm{d}x, \tag{30}$$

where $e_0, e_1, \ldots, e_{M+1}$ are the hat functions introduced in Section 2.3.2.

After some algebraic manipulations, we obtain

$$\hat{\mathsf{A}} = \frac{D_0}{h}\begin{bmatrix} r_1 & q_1 & 0 & 0 & \cdots & \cdots & 0 \\ q_1 & r_2 & q_2 & 0 & \cdots & \cdots & 0 \\ 0 & \ddots & \ddots & \ddots & \ddots & & 0 \\ \vdots & \ddots & \ddots & \ddots & \ddots & \ddots & \vdots \\ 0 & \cdots & 0 & q_{M-3} & r_{M-2} & q_{M-2} & 0 \\ 0 & \cdots & \cdots & 0 & q_{M-2} & r_{M-1} & q_{M-1} \\ 0 & \cdots & \cdots & 0 & 0 & q_{M-1} & r_M \end{bmatrix},$$

with matrix components depending on the value of k. Specifically, for $k = 1$,

$$q_i := -1 - \frac{\delta}{2h}(\alpha_i^n + \alpha_{i+1}^n),$$
$$r_i := 2 + \frac{\delta}{2h}(\alpha_{i-1}^n + 2\alpha_i^n + \alpha_{i+1}^n),$$

while for $k = 2$,

$$q_i := -\frac{1}{3}(1+\delta\alpha_i)^2 - \frac{1}{3}(1+\delta\alpha_i)(1+\delta\alpha_{i+1}) - \frac{1}{3}(1+\delta\alpha_{i+1})^2,$$
$$r_i := \frac{1}{3}(1+\delta\alpha_{i-1})^2 + \frac{2}{3}(1+\delta\alpha_i)^2 + \frac{1}{3}(1+\delta\alpha_{i+1})^2 + \frac{1}{3}(1+\delta\alpha_i)(2+\delta\alpha_{i-1}+\delta\alpha_{i+1}).$$

Finally, for each $n \in \{0, 1, \ldots, N\}$, we set $\mu^{n+1} \in \mathbb{R}^M$ as the vector whose components are all zero, except for the first and last ones, which are set to ϕ_∞^{n+1}. Then, the matrix form of (26) reads as follows: for each $n \in \{0, 1, \ldots, N\}$, find $\alpha^{n+1} := (\alpha_j^{n+1}) \in \mathbb{R}^M$ such that

$$(\mathsf{B} + \Delta t^n \hat{\mathsf{A}})\alpha^{n+1} = \mathsf{B}\alpha^n - (\mathsf{B} + \Delta t^n \hat{\mathsf{A}})\mu^{n+1}, \tag{31}$$

where the matrix B is defined as in Section 2.3.2.

Remark 2. *The unique solvability of the fully discrete scheme* (31) *follows from the fact that the diffusion coefficient* (28) *satisfies the condition* (29). *In fact, the matrix* $\mathsf{B} + \Delta t^n \hat{\mathsf{A}}$ *is symmetric, and for any vector* $\beta \in \mathbb{R}^M$ *given by* (20), *we have*

$$\beta^T(\mathsf{B} + \Delta t^n \hat{\mathsf{A}})\beta \geq \Delta t^n C \|\psi_h\|_{1,I}^2,$$

with constant $C > 0$ *depending on* D_* *and the constant from Poincaré's inequality. It then follows that the matrix* $\mathsf{B} + \Delta t^n \hat{\mathsf{A}}$ *is positive definite, and therefore invertible.*

3. Results

3.1. Drug Release Experiments

Samples of NC/nPSi composites (0.5 × 0.5 cm^2) with varying concentrations of microparticulate nPSi were synthesized following the protocol outlined by K. Garrido-Miranda et al. [12]. Each sample had different thicknesses based on the percentage of nPSi (m/m): NC (control, 0.0%) = 6.5 ± 1 µm, NC/nPSi-0.1% = 10.5 ± 2 µm, NC/nPSi-0.5% = 12.7 ± 3 µm, and NC/nPSi-1.0% = 29.5 ± 4 µm (Figure 3). Subsequently, the samples were loaded with a concentrated MB solution (0.001 M, pH 7.0) for 15 min at 100 rpm. They were then rinsed with distilled water and dried at room temperature. Release pro-

files were conducted in vials filled with 3 ml of saline phosphate-buffered solution (PBS, pH 7 and 37 °C) at 100 rpm on a horizontal shaker (INB-2005 LN, Biotek, Winooski, VT, USA). The concentration of MB in the fluid was measured at specific time intervals using UV-Vis spectrophotometry (UV-1800 Shimadzu, Kyoto, Japan) at a wavelength of 671 nm [7]. The release profiles were obtained as the mean of triplicate experiments (see the Supplementary Materials section).

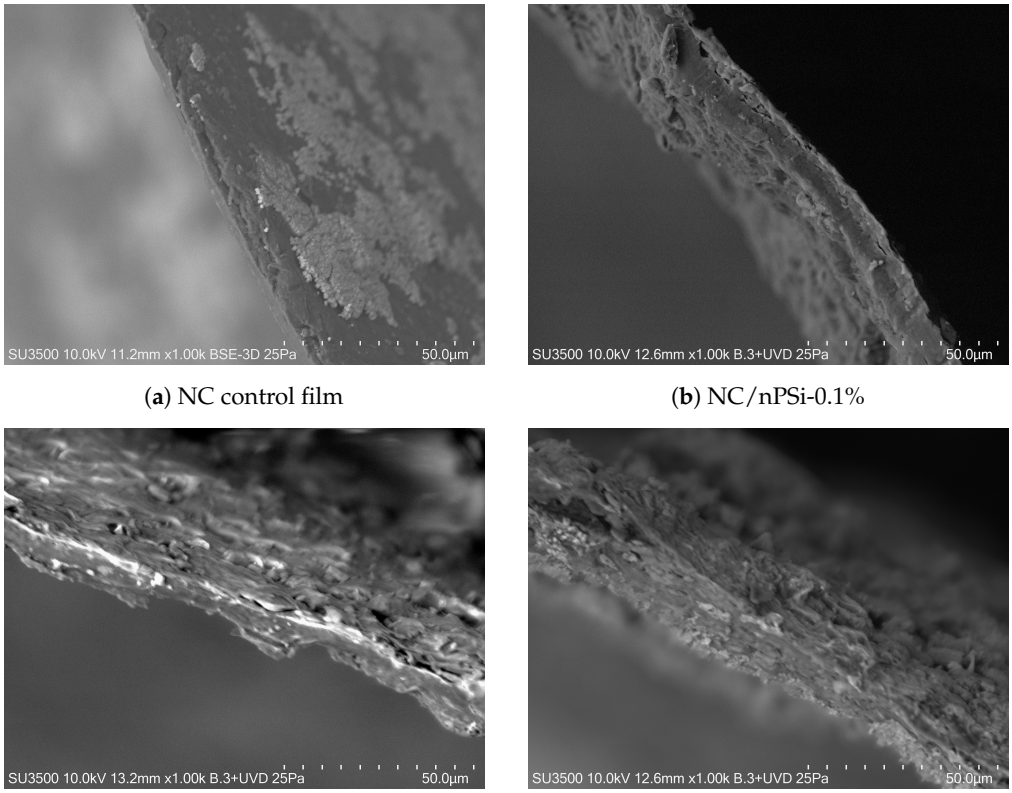

(**a**) NC control film (**b**) NC/nPSi-0.1%

(**c**) NC/nPSi-0.5% (**d**) NC/nPSi-1.0%

Figure 3. SEM images of samples.

3.2. Model Prediction

In this section, we compare the drug release experiments with the numerical results obtained using the FE method described in Section 2.4. All simulations were implemented using Octave 8.4.0 [33].

In what follows, the diffusion coefficient D is defined as in (28), with the constant D_0 determined using the Nelder–Mead optimization method [41], which minimizes the error

$$e_{ana} := \sqrt{\sum_{n=0}^{N+1} \left| u^n - w^n(D_0) \right|^2},$$

where u^n represents the experimental release profile at time t^n, and $w^n(D_0)$ denotes the corresponding value obtained from the analytical release profile in (3), computed as

$$w^n(D_0) = 1 - \frac{8}{\pi^2} \sum_{k=0}^{p} \frac{1}{(2k+1)^2} \exp\left[-\frac{D_0 (2k+1)^2 \pi^2 t^n}{4L^2} \right].$$

Note here that p is a user-defined integer, which we set to $p = 100$. The computed values of D_0 for the four samples detailed in Section 3.1 are listed in Table 1. Once the parameter D_0 is determined, we proceed to complete the definition of the diffusion coef-

ficient D by selecting an appropriate value for the scalar δ, as will be discussed in more detail below. With D being fully defined, the release profile M_t/M_∞ is approximated by solving Fick's second law using the FE method. Specifically, the solution to the system (31), as obtained from Algorithm 1, provides the following approximation:

$$\left.\frac{M_t}{M_\infty}\right|_{t=t^{n+1}} \approx \frac{\int_{-L}^{L}(\phi_h^{n+1}-\phi_0)\,\mathrm{d}x}{\int_{-L}^{L}(\phi_\infty^{n+1}-\phi_0)\,\mathrm{d}x}. \tag{32}$$

Unless otherwise specified, we choose $\phi_0 = 1$ and $\phi_\infty^{n+1} = 0$ for all $n \in \{0, 1, \ldots, N+1\}$.

Table 1. Computed values of D_0.

Sample	D_0 (μm²/h)
NC	28.648
NC/nPSi-0.1%	107.640
NC/nPSi-0.5%	17.413
NC/nPSi-1.0%	51.523

Algorithm 1 FE solution.

Input: N, M, δ, D_{ref}, ϕ_0, ϕ_∞, L
Output: $\phi_h^0, \phi_h^1, \ldots, \phi_h^{N+1}$

$h \leftarrow 2L/(M+1)$
$\phi_h^0 \leftarrow L^2$-projection of ϕ_0 into V_h (cf. (14))
for $n = 0, 1, \ldots, N$ **do**
  $\Delta t^n \leftarrow t^{n+1} - t^n$
  $\alpha_0^{n+1} \leftarrow \phi_\infty^{n+1}$
  $\alpha_{M+1}^{n+1} \leftarrow \phi_\infty^{n+1}$
  $\alpha_1^{n+1}, \ldots, \alpha_M^{n+1} \leftarrow$ solution to the problem (31)
  $\phi_h^{n+1} \leftarrow \sum_{j=0}^{M+1} \alpha_j^{n+1} e_j$

Selecting the optimal values for δ and k is essential for accurately defining the diffusion coefficient D. To determine these values, we focused on the samples in Table 1. For each sample, k was set to either 1 or 2, the meshsize h was computed as $2L/(M+1)$ with $M = 31$, and δ was chosen from the interval $[-1, 1]$. The goal was to minimize the numerical error

$$e_{num} := \sqrt{\sum_{n=0}^{N+1} \left|u^n - v^n(\delta)\right|^2}, \tag{33}$$

where the experimental release profile at time t^n is denoted by u^n, while $v^n(\delta)$ represents the corresponding approximation from (32). Values of δ outside the interval $[-1, 1]$ led to larger errors and were therefore discarded. In this context, the computed errors for $k = 2$ are shown in Table 2, indicating that the optimal value of δ is 0.3 for the first three samples and 0.2 for the last one. Thus, condition (29) is satisfied with $D_* = D_0$, ensuring the unique solvability of the fully discrete scheme (26), as stated in Remark 2. Similar results for $k = 1$ were obtained and are omitted for brevity.

Table 2. Release profile of errors associated with the variable diffusion coefficient D for $k = 2$.

NC							
δ	-1	-0.3	-0.2	0	0.2	0.3	1
e_{num}	1.636	0.320	0.262	0.166	0.104	0.092	0.200
e_{ana}	–	–	–	0.140	–	–	–
NC/nPSi-0.1%							
δ	-1	-0.3	-0.2	0	0.2	0.3	1
e_{num}	1.573	0.333	0.279	0.194	0.145	0.135	0.193
e_{ana}	–	–	–	0.178	–	–	–
NC/nPSi-0.5%							
δ	-1	-0.3	-0.2	0	0.2	0.3	1
e_{num}	1.344	0.314	0.264	0.185	0.141	0.134	0.263
e_{ana}	–	–	–	0.171	–	–	–
NC/nPSi-1.0%							
δ	-1	-0.3	-0.2	0	0.2	0.3	1
e_{num}	1.219	0.306	0.257	0.191	0.176	0.185	0.351
e_{ana}	–	–	–	0.146	–	–	–

Figure 4 shows the experimental release data, their numerical approximations using the FE method, and the analytical solution from (3). The FE solution provided the best fit for the experimental data in the first three samples. For the last sample, where the concentration of nPSi was higher, the analytical release profile was 20.55% more accurate, as indicated by the errors in Table 2. It follows that D strongly depends on the concentration when the percentage of nPSi is below 1.0%. Additionally, the simulations in Figure 5 reveal that the diffusion rate decreases at higher nPSi percentages, as reflected by the slower reduction in concentration across the thickness, particularly in the last sample. These results align with the experimental findings of K. Garrido-Miranda et al. [12], where incorporating nPSi into the material enhances control over the release of MB.

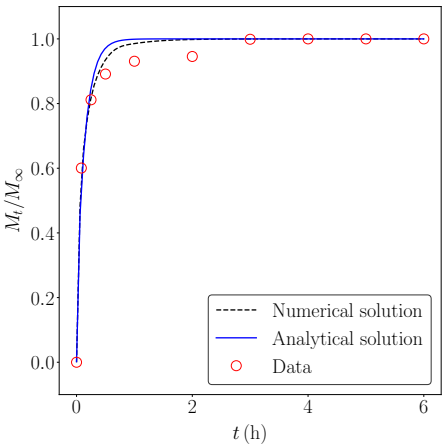

(**a**) NC: $k = 2$ and $\delta = 0.3$

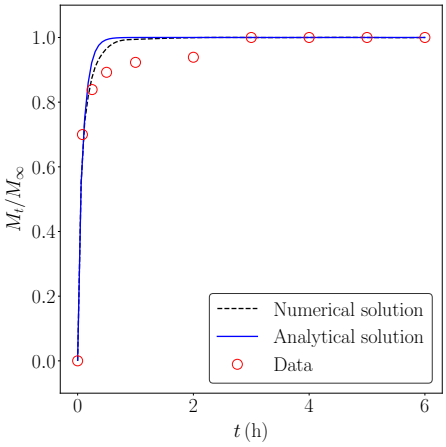

(**b**) NC/nPSi-0.1%: $k = 2$ and $\delta = 0.3$

Figure 4. *Cont.*

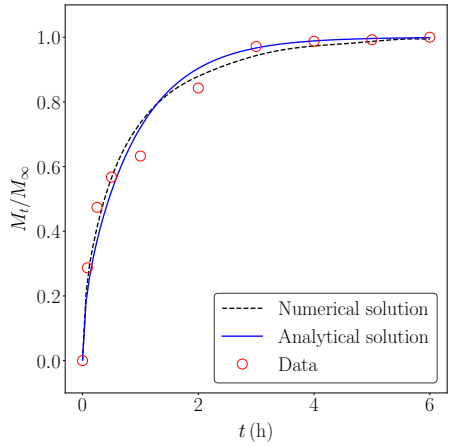

(**c**) NC/nPSi-0.5%: $k = 2$ and $\delta = 0.3$

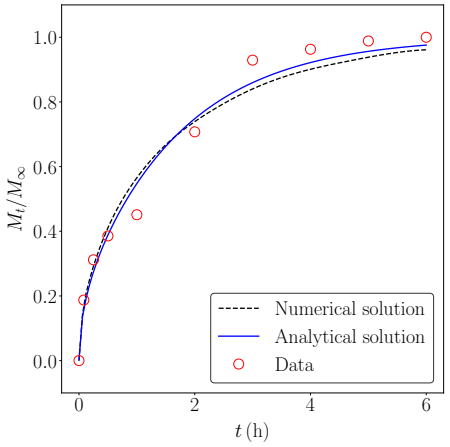

(**d**) NC/nPSi-1.0%: $k = 2$ and $\delta = 0.2$

Figure 4. Numerical vs. analytical drug release profiles.

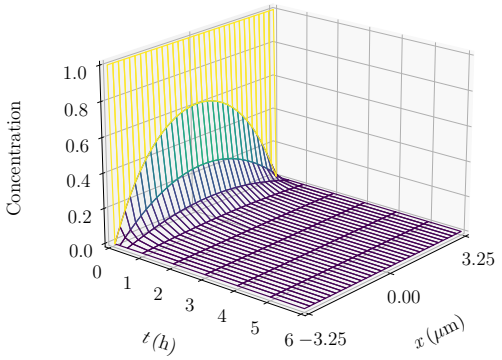

(**a**) NC: $k = 2$ and $\delta = 0.3$

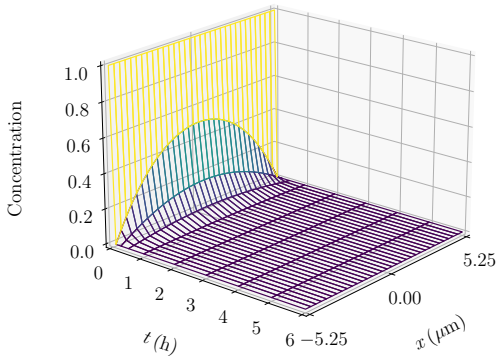

(**b**) NC/nPSi-0.1%: $k = 2$ and $\delta = 0.3$

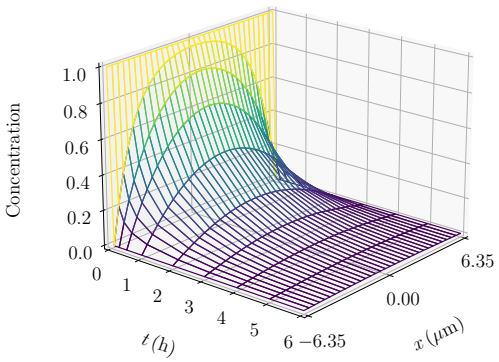

(**c**) NC/nPSi-0.5%: $k = 2$ and $\delta = 0.3$

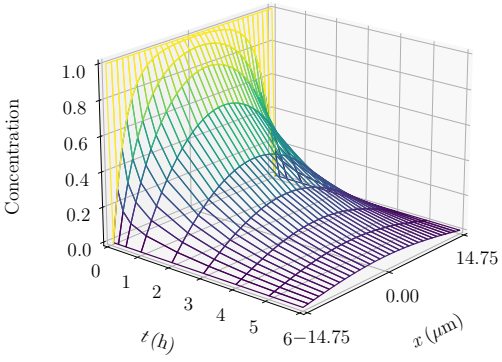

(**d**) NC/nPSi-1.0%: $k = 2$ and $\delta = 0.2$

Figure 5. Approximate concentration.

4. Discussion

The FE method presented in Section 2.4 provides a general framework for accurately describing the drug delivery system under consideration. In fact, the variable diffusion coefficient defined in (28) showed strong agreement with data from K. Garrido-Miranda et al. [12], particularly for samples with nPSi percentages below 1.0%. A weaker dependency was observed at an nPSi concentration of exactly 1.0%. This may be linked to the increased thickness associated with higher nPSi levels, which was presumed negligible in both the numerical method and the analytical solution.

In our simulations, we assumed constant initial and boundary conditions. However, a more realistic assumption would involve time-dependent boundary data, which may occur

when the solution is not well stirred [42]. Notably, the fully discrete scheme (26) remains effective in simulating this scenario, as illustrated in Figure 6 for a single sample, where the boundary data were derived from the empirical relation $\phi_\infty(t) = 1 - M_t/M_\infty$. These results were contrasted with the analytical solution from (3), showing that the numerical solution with time-dependent ϕ_∞ performs better when $M_t/M_\infty < 0.85$. This conclusion is further supported by the error computed from (33) using $\delta = 0.45$ and $k = 2$, yielding a value of 0.149, which represents a 14.77% improvement compared to the corresponding error reported in Table 2 for the analytical solution with constant boundary conditions.

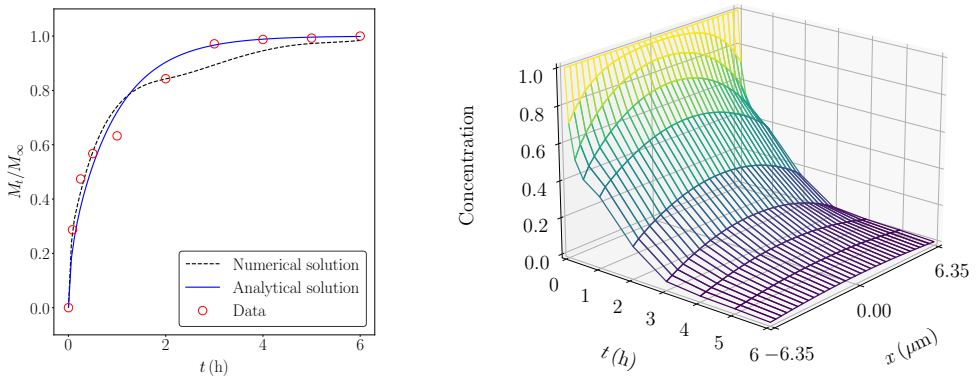

(**a**) Numerical vs. analytical drug release profiles (**b**) Approximate concentration

Figure 6. NC/nPSi-0.5%: $k = 2$ and $\delta = 0.45$.

Building on these results, a more comprehensive approach to designing drug delivery systems that undergo significant geometric changes and time-dependent boundary conditions should incorporate space–time FE methods (see, e.g., [43,44]). Future work will explore this approach by incorporating additional parameters into the general form of diffusion coefficient presented in Remark 1, with the aim of capturing effects such as evaporation within the composite.

5. Conclusions

This study employed an FE method to model diffusion and controlled drug release from NC/nPSi composites based on Fick's second law with variable diffusivity. The FE simulations, supported by experimental validation, demonstrated that increasing the nPSi concentration in the NC matrix enhances control over the release MB. This finding is particularly relevant for pharmaceutical applications, where controlled drug delivery is critical to minimize adverse effects on tissues. Furthermore, this study highlights the importance of considering geometric changes in the composite matrix, especially at high nPSi concentrations, which significantly influence drug release behavior. Addressing these complexities is a priority for future work to extend the applicability of the proposed model to a wider range of material configurations and drug delivery scenarios. The results not only validate the effectiveness of the FE method for modeling diffusion in composite materials but also provide insights into optimizing the design of NC/nPSi composites for controlled drug release. This work sets a foundation for further research into more complex geometries and dynamic environmental conditions, reinforcing its potential contributions to the development of advanced drug delivery systems.

Supplementary Materials: The following supporting information can be downloaded at https://www.mdpi.com/article/10.3390/pharmaceutics17010120/s1, Table S1: Experimental MB release data from NC/nPSi composites; Table S2: Cumulative release of MB.

Author Contributions: Conceptualization, P.Z., M.A. and J.H.-M.; methodology, P.Z., M.A., S.P. and J.H.-M.; software, P.Z. and M.A.; validation, P.Z. and J.H.-M.; formal analysis, P.Z. and M.A.; resources, P.Z., S.P. and J.H.-M.; data curation, P.Z. and M.A.; writing—original draft preparation, P.Z. and J.H.-M.; funding acquisition, J.H.-M. All authors have read and agreed to the published version of the manuscript.

Funding: This research was funded by FONDECYT, Chile, grant numbers 11180395 and 1230553.

Institutional Review Board Statement: Not applicable.

Informed Consent Statement: Not applicable.

Data Availability Statement: The data presented in this study are available in the Supplementary Materials.

Acknowledgments: M.A. acknowledges support from the Master in Applied Mathematics program at UC-Temuco, Chile, and the Master for Educational Professionals ANID Grant No. 50210068, Chile.

Conflicts of Interest: The authors declare no conflicts of interest.

References

1. Guo, K.W. Nanoporous Silicon Materials for Bioapplications by Electrochemical Approach. In *Nanobiomaterials*; CRC Press: Boca Raton, FL, USA, 2024; pp. 188–196.
2. Jung, Y.; Huh, Y.; Kim, D. Recent advances in surface engineering of porous silicon nanomaterials for biomedical applications. *Microporous Mesoporous Mater.* **2021**, *310*, 110673. [CrossRef]
3. Coffer, J.L.; Canham, L.T. Nanoporous silicon as a green, high-tech educational tool. *Nanomaterials* **2021**, *11*, 553. [CrossRef] [PubMed]
4. Hernandez-Montelongo, J.; Naveas, N.; Degoutin, S.; Tabary, N.; Chai, F.; Spampinato, V.; Ceccone, G.; Rossi, F.; Torres-Costa, V.; Manso-Silvan, M.; et al. Porous silicon-cyclodextrin based polymer composites for drug delivery applications. *Carbohydr. Polym.* **2014**, *110*, 238–252. [CrossRef] [PubMed]
5. Anglin, E.J.; Cheng, L.; Freeman, W.R.; Sailor, M.J. Porous silicon in drug delivery devices and materials. *Adv. Drug Deliv. Rev.* **2008**, *60*, 1266–1277. [CrossRef] [PubMed]
6. Guzmán-Oyarzo, D.; Hernández-Montelongo, J.; Rosas, C.; Leal, P.; Weber, H.; Alvear, M.; Salazar, L.A. Controlled release of caffeic acid and pinocembrin by use of nPSi-βCD composites improves their antiangiogenic activity. *Pharmaceutics* **2022**, *14*, 484. [CrossRef]
7. Hernández-Montelongo, J.; Oria, L.; Cardenas, A.B.; Benito, N.; Romero-Sáez, M.; Recio-Sánchez, G. Nanoporous silicon composite as potential system for sustained delivery of florfenicol drug. *Phys. Status Solidi (b)* **2018**, *255*, 1700626. [CrossRef]
8. Franca, C.G.; Plaza, T.; Naveas, N.; Santana, M.H.A.; Manso-Silván, M.; Recio, G.; Hernandez-Montelongo, J. Nanoporous silicon microparticles embedded into oxidized hyaluronic acid/adipic acid dihydrazide hydrogel for enhanced controlled drug delivery. *Microporous Mesoporous Mater.* **2021**, *310*, 110634. [CrossRef]
9. McInnes, S.J.; Irani, Y.; Williams, K.A.; Voelcker, N.H. Controlled drug delivery from composites of nanostructured porous silicon and poly (L-lactide). *Nanomedicine* **2012**, *7*, 995–1016. [CrossRef]
10. Thomas, B.; Raj, M.C.; Joy, J.; Moores, A.; Drisko, G.L.; Sanchez, C. Nanocellulose, a versatile green platform: From biosources to materials and their applications. *Chem. Rev.* **2018**, *118*, 11575–11625. [CrossRef]
11. Huo, Y.; Liu, Y.; Xia, M.; Du, H.; Lin, Z.; Li, B.; Liu, H. Nanocellulose-based composite materials used in drug delivery systems. *Polymers* **2022**, *14*, 2648. [CrossRef]
12. Garrido-Miranda, K.A.; Pesenti, H.; Contreras, A.; Vergara-Figueroa, J.; Recio-Sánchez, G.; Chumpitaz, D.; Ponce, S.; Hernandez-Montelongo, J. Nanocellulose/Nanoporous Silicon Composite Films as a Drug Delivery System. *Polymers* **2024**, *16*, 2055. [CrossRef] [PubMed]
13. Jack Clifton, I.; Leikin, J.B. Methylene blue. *Am. J. Ther.* **2003**, *10*, 289–291. [CrossRef] [PubMed]
14. Cwalinski, T.; Polom, W.; Marano, L.; Roviello, G.; D'Angelo, A.; Cwalina, N.; Matuszewski, M.; Roviello, F.; Jaskiewicz, J.; Polom, K. Methylene blue—Current knowledge, fluorescent properties, and its future use. *J. Clin. Med.* **2020**, *9*, 3538. [CrossRef] [PubMed]
15. Lee, S.W.; Han, H.C. Methylene blue application to lessen pain: Its analgesic effect and mechanism. *Front. Neurosci.* **2021**, *15*, 663650. [CrossRef]
16. Sahu, A.; Choi, W.I.; Lee, J.H.; Tae, G. Graphene oxide mediated delivery of methylene blue for combined photodynamic and photothermal therapy. *Biomaterials* **2013**, *34*, 6239–6248. [CrossRef]
17. Brenner, S.C.; Scott, L.R. *The Mathematical Theory of Finite Element Methods*, 3rd ed.; Springer: Berlin/Heidelberg, Germany, 2010.
18. Ciarlet, P.G. *The Finite Element Method for Elliptic Problems*; SIAM: Philadelphia, PA, USA, 2002.

19. Girault, V.; Raviart, P.A. *Finite Element Methods for Navier-Stokes Equations: Theory and Algorithms*; Volume 5, Springer Series in Computational Mathematics; Springer: Berlin, Germany, 1986.
20. Teixeira, P.R.d.F.; Awruch, A.M. Numerical simulation of fluid–structure interaction using the finite element method. *Comput. Fluids* **2005**, *34*, 249–273. [CrossRef]
21. Monk, P. *Finite Element Methods for Maxwell's Equations*; Oxford University Press: Oxford, UK, 2003.
22. Oyarzúa, R.; Zúñiga, P. Analysis of a conforming finite element method for the Boussinesq problem with temperature-dependent parameters. *J. Comput. Appl. Math.* **2017**, *323*, 71–94. [CrossRef]
23. Fick, A. Ueber diffusion. *Ann. Der Phys.* **1855**, *170*, 59–86. [CrossRef]
24. Aguerre, R.; Gabitto, J.; Chirife, J. Utilization of Fick's second law for the evaluation of diffusion coefficients in food processes controlled by internal diffusion. *Int. J. Food Sci. Technol.* **1985**, *20*, 623–629. [CrossRef]
25. Hernandez-Montelongo, R.; Salazar-Araya, J.; Hernandez-Montelongo, J.; Garcia-Sandoval, J.P. Mathematical modeling of recursive drug delivery with diffusion, equilibrium, and convection coupling. *Mathematics* **2022**, *10*, 2171. [CrossRef]
26. Lavery, P.S.; Oldham, C.E.; Ghisalberti, M. The use of Fick's First Law for predicting porewater nutrient fluxes under diffusive conditions. *Hydrol. Process.* **2001**, *15*, 2435–2451. [CrossRef]
27. Ochoa-Martínez, C.; Ramaswamy, H.; Ayala-Aponte, A. Suitability of Crank's solutions to Fick's second law for water diffusivity calculation and moisture loss prediction in osmotic dehydration of fruits. *J. Food Process Eng.* **2009**, *32*, 933–943. [CrossRef]
28. Shi, S.Q. Diffusion model based on Fick's second law for the moisture absorption process in wood fiber-based composites: Is it suitable or not? *Wood Sci. Technol.* **2007**, *41*, 645–658. [CrossRef]
29. Terazima, M. Diffusion coefficients as a monitor of reaction kinetics of biological molecules. *Phys. Chem. Chem. Phys.* **2006**, *8*, 545–557. [CrossRef] [PubMed]
30. Falk, B.; Garramone, S.; Shivkumar, S. Diffusion coefficient of paracetamol in a chitosan hydrogel. *Mater. Lett.* **2004**, *58*, 3261–3265. [CrossRef]
31. García-González, C.A.; Sosnik, A.; Kalmár, J.; De Marco, I.; Erkey, C.; Concheiro, A.; Alvarez-Lorenzo, C. Aerogels in drug delivery: From design to application. *J. Control. Release* **2021**, *332*, 40–63. [CrossRef]
32. Ash, R.; Espenhahn, S.E. Transport through a slab membrane governed by a concentration-dependent diffusion coefficient. Part I. The four time-lags: Some general considerations. *J. Membr. Sci.* **1999**, *154*, 105–119. [CrossRef]
33. Eaton, J.W.; Bateman, D.; Hauberg, S.; Wehbring, R. GNU Octave Version 8.4.0 Manual: A High-Level Interactive Language for Numerical Computations. 2023. Available online: https://docs.octave.org/v8.4.0/ (accessed on 14 December 2024).
34. Crank, J. *The Mathematics of Diffusion*; Oxford University Press: Oxford, UK, 1979.
35. Brezis, H. *Functional Analysis, Sobolev Spaces and Partial Differential Equations*; Springer: New York, NY, USA, 2011.
36. Braess, D. *Finite Elements: Theory, Fast Solvers, and Applications in Solid Mechanics*; Cambridge University Press: Cambridge, UK, 2007.
37. Ern, A.; Guermond, J.L. *Theory and Practice of Finite Elements*; Springer: Berlin/Heidelberg, Germany, 2004; Volume 159.
38. Quarteroni, A.; Sacco, R.; Saleri, F. *Numerical Mathematics*; Springer Science & Business Media: Berlin/Heidelberg, Germany, 2006; Volume 37.
39. Crank, J.; Henry, M. Diffusion in media with variable properties. Part I. The effect of a variable diffusion coefficient on the rates of absorption and desorption. *Trans. Faraday Soc.* **1949**, *45*, 636–650. [CrossRef]
40. Clément, R.; Nguyen, Q.T.; Grosse, J.M.; Uchytil, P. Simulation and modelling of transient permeation of organic solvents through polymer films in the case of a concentration dependent diffusion coefficient. *Macromol. Theory Simul.* **1995**, *4*, 921–933. [CrossRef]
41. Nelder, J.A.; Mead, R. A Simplex Method for Function Minimization. *Comput. J.* **1965**, *7*, 308–313. [CrossRef]
42. Vergnaud, J.M. *Controlled Drug Release of Oral Dosage Forms*; CRC Press: Boca Raton, FL, USA, 1993.
43. Langer, U.; Neumüller, M.; Schafelner, A. Space-time finite element methods for parabolic evolution problems with variable coefficients. In *Advanced Finite Element Methods with Applications: Selected Papers from the 30th Chemnitz Finite Element Symposium 2017*; Springer: Berlin/Heidelberg, Germany, 2019, pp. 247–275.
44. Steinbach, O. Space-time finite element methods for parabolic problems. *Comput. Methods Appl. Math.* **2015**, *15*, 551–566. [CrossRef]